Advanced Composites and Hybrid Materials (2025) 8:393
https://doi.org/10.1007/s42114-025-01481-0

RESEARCH

Polymer dispersed liquid crystals-impregnated switchable thermochromic transparent woods with excellent ultraviolet blocking performance for smart windows

Cheng Ai Li[1] · Jae Gyu Ahn[1] · Hyeon Ji Jeong[1] · Jang Hee Kim[1] · Taeyoung Park[1] · Do Kyoung Han[2,3] · Jin Kim[4] · Dong Ju Lee[5] · Sung Ho Song[1]

Received: 10 July 2025 / Revised: 17 September 2025 / Accepted: 19 September 2025
© The Author(s) 2025

Abstract

Due to the damage caused by ultraviolet (UV) radiations, the development of smart windows with UV-shielding capability is urgently needed to help reduce the aging of household items and protect human health. Traditional glasses exhibit inferior UV- and heat-shielding properties. Therefore, constructing alternative materials with high transparencies, low thermal conductivities, and excellent UV-blocking capabilities is significantly important to replace traditional glasses. Herein, switchable thermochromic transparent woods (TWs) are fabricated for smart windows using UV-curable polymer dispersed liquid crystal (PDLC) into modified woods for the first time. Thermochromic TW filled with PDLC (PDLC/TW) adjusts its visible light transmittance based on temperature without additional energy. Balsa PDLC/TW demonstrates a gradually increasing transmittance (from 28% at room temperature to 78% at 40 °C) at 550 nm. Moreover, balsa PDLC/TW exhibits outstanding UV-blocking performance and almost five times lower thermal conductivity (0.197 W m^{-1} K^{-1}) than that of the glass (0.911 W m^{-1} K^{-1}). As-prepared PDLC/TWs can effectively allow the passage of visible light and block UV light during the day, which is beneficial for indoor illumination and human health. Interestingly, at night, they become opaque, thereby protecting privacy. These findings highlight the considerable potentials of PDLC/TWs for application in next-generation energy-efficient buildings.

Keywords Transparent wood · Thermochromic polymer-dispersed liquid crystals · UV blocking · Smart windows

1 Introduction

Environmentally friendly and energy-efficient buildings are particularly attractive for sustainable development and energy consumption in accordance with environmental, social, and energetic criteria [1–3]. With the rapid rise in

Cheng Ai Li and Jae Gyu Ahn contributed equally to this work.

✉ Jin Kim
jinnie.kim@hanbat.ac.kr

✉ Dong Ju Lee
dongjulee@chungbuk.ac.kr

✉ Sung Ho Song
shsong805@kongju.ac.kr

[1] Division of Advanced Materials Engineering, Center for Advanced Materials and Parts of Powders, Kongju National University, Cheonan-Si 31080, Republic of Korea

[2] Division of Materials Analysis and Research, Korea Basic Science Institute, 169–148, Gwahak-Ro, Yuseong-Gu, Daejeon 34133, Republic of Korea

[3] Department of Chemistry, Chung-Ang University, Seoul 06974, Republic of Korea

[4] Department of Materials Science and Engineering, Hanbat National University, Daejeon 34158, Republic of Korea

[5] Department of Urban, Energy, and Environmental Engineering, Chungbuk National University, Cheongju 28644, Republic of Korea

Published online: 16 October 2025

energy consumption due to the construction of new buildings and improved living standards, considerable efforts have been made to develop smart windows with multi-features, such as optical modulation and energy efficiency, to replace conventional glass windows [4–7]. Additionally, ozone depletion and increase in ultraviolet (UV) radiation on the ground poses risks to human health and accelerate the discoloration of indoor materials [8–10]. Therefore, the development smart windows with UV-shielding capabilities is urgently needed to help reduce the aging of household items and protect human health. Smart windows can regulate the amount of sunlight entering buildings, providing a comfortable environment for people on demand while also facilitating energy conservation. Currently, self-powered smart windows that utilize green energy to achieve energy savings and support environmental protection are significant required [11, 12]. Among them, thermochromic windows are regarded as cost-effective energy-saving smart windows because they can control light without requiring energy inputs [4, 6, 12–14]. These windows use thermochromic materials that undergo reversible phase transitions between transparent and opaque states in response to temperature variations. Adjusting transparency based on temperature not only can decrease glare and heat gain from strong sunlight, but can also ensure privacy by preventing outside views.

Polymer dispersed liquid crystals (LCs) (PDLCs) are a type of smart materials in which LCs are embedded in a continuous polymer matrix. Thermochromic LC-based smart windows switch between transparent and opaque states according to temperature, enabling the regulation of light and heat entering the building [15–17]. For thermochromic PDLC-based smart windows, the ideal design should remain opaque at lower temperature at night and become transparent at higher temperature during the day, ensuring indoor lighting during the day while maintaining privacy at night. However, many PDLC materials only function effectively under visible light and lack modulation capabilities under UV light [18–22]. In recent decades, optically transparent organic/inorganic UV-absorbers composite thin films have been developed to protect against UV light [18, 22–26]. Nevertheless, during application to windows, these films must be coated on glass or placed between two glass panels, which can be fragile, costly, and unsafe. Furthermore, because of the high thermal conductivity and inferior heat-shielding properties of glass, a substantial amount of energy is wasted in heating or cooling buildings via inefficient windows. Thus, creating alternative materials with high transparencies, low thermal conductivities, and excellent UV-blocking capabilities is significantly important for replacing traditional architectural glass.

Recently, transparent wood (TW) has been investigated as a biocomposite material that demonstrates comparable optical transmittance to that of traditional architectural glass, effective thermal insulation, and outstanding mechanical properties, rendering it suitable for use in energy-efficient buildings and smart windows [1, 2, 5, 6, 27–29]. Wood serves as a raw material and has significantly contributed to the development of sustainable functional TWs due to its abundant availability, eco-friendly properties, ease of processing, low thermal conductivity, and high mechanical performance [3, 30, 31]. Hierarchical structure and strong interactions among cellulose, hemicelluloses, and lignin endow wood with excellent mechanical properties. However, chromophore groups in lignin impart a brownish color to natural wood (NW), rendering it unsuitable for application in transparent materials and smart windows [23, 25]. Typically, TW is mainly fabricated by removing or modifying lignin in wood, followed by filling the wood template with refractive index-matching polymers including epoxy resin, polymethylmethacrylate, polyvinyl alcohol, and polyvinylpyrrolidone [2, 5, 27, 32–38]. Properties and functions of TWs are influenced by the characteristics of the embedded polymers and additives. For instance, the incorporating of quantum dots or dyes into polymers can create functional TWs appropriate for use in smart windows and optical devices [34–36]. An approach to advance current research on TWs for smart window applications is to endow TWs with abilities to manipulate their optical properties in response to environmental conditions. To the best of our knowledge, research on thermally switchable TWs that exhibit phase transitions and reversible transparent-to-opaque transitions with respect to temperature is still limited. Additionally, to date, a thermochromic TW with UV-blocking capabilities has not been explored. Although studies on TWs with thermochromic additives have been reported, these TWs do not provide UV protection [5, 39–41]. Thus, our aim is to develop thermochromic TW that is both temperature-responsive and capable of offering shielding against UV light for smart windows.

In this study, we synthesized switchable thermochromic TWs by infiltrating UV-curable PDLCs into the modified woods to control the optical modulation performance of these woods and offer UV-shielding functionalities without adding UV-absorbing components. We identified three common wood species (namely, balsa, bass, and pine woods) as raw wood materials for preparing thermochromic TWs filled with PDLC (PDLC/TWs). At first, the woods were lignin modified followed by bleaching, and then, the bleached woods (BWs) were impregnated with a mixture of thermochromic LC (4-cyano-4'-*n*-octylbiphenyl, 8CB) and UV-cured Norland Optical Adhesives (NOAs) (NOA 63) followed by polymerization using UV light. With an increase in temperature from below room temperature (RT) to 40 °C, as-fabricated PDLC/TWs changed stepwise from the opaque phase to the translucent phase and finally reached the transparent phases. Below RT, balsa PDLC/TW demonstrated

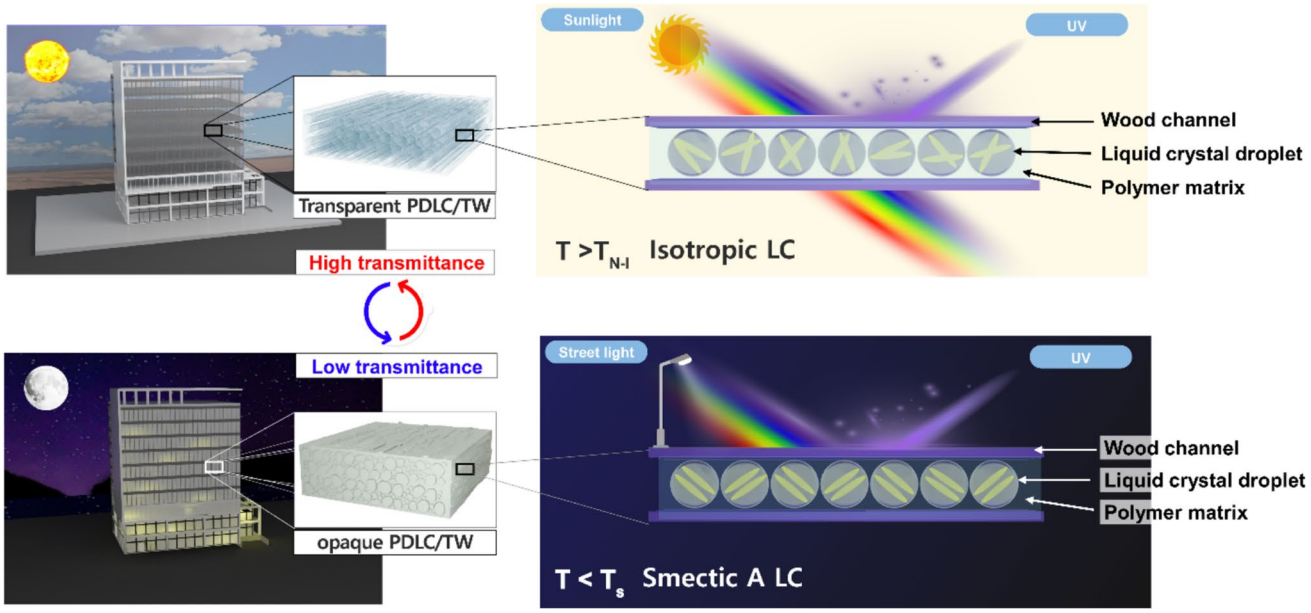


Fig. 1 Schematic of the reversible transparent-to-opaque phase transition of PDLC/TW in response to temperature variations. During the day, PDLC/TW becomes transparent due to the substrate temperature above the temperature for nematic-to-isotropic (T_{N-I}) transition of liquid crystals (8CB), allowing visible light to enter and blocking UV radiations. In contrast, at night, PDLC/TW turns opaque owing to the substrate temperature below the phase transition temperature of the smectic A phase (Ts) of the liquid crystals, thereby blocking visible light and ensuring customer privacy

a transmittance of 28% at 550 nm, which increased to 78% above 40 °C. Alteration in transmittance was accomplished by incorporating 8CB into PDLC/TWs that exhibits different phases at various temperatures. Furthermore, transparent balsa PDLC/TW blocked most of the UV light in the wavelength range of 320–400 nm. It also demonstrated excellent thermal insulation property (0.197 W m^{-1} K^{-1}) as compared to that of conventional glass (0.911 W m^{-1} K^{-1}), rendering it highly beneficial for thermal insulation and effectively reducing energy loss. As shown in Fig. 1, during the day, PDLC/TW as a smart window material is in a transparent phase, allowing light to pass through it for indoor illumination. Moreover, it blocks UV light, which is advantageous for both indoor lighting and human health. At night, as-prepared PDLC/TW transforms to an opaque phase with low transmittance, thereby ensuring customer privacy. PDLC/TW can overcome the limitations of glass, functioning as a smart window material that offers intelligent and efficient optical regulation to reduce high energy consumption in buildings. We also utilized thin PDLC/TW as a wearable temperature sensor that could track human body temperature, exhibiting considerable promise for adaptable and energy-autonomous next-generation wearable devices.

2 Experimental section

Materials and chemicals Balsa and bass woods were purchased from Midwest products, USA, and pine wood was obtained from a local market in South Korea. Slices with sizes of 20 × 20 × 2 mm^3 (longitudinal × radial × tangential, respectively) from balsa, bass, and pine woods were cut parallel to the tree growth direction. Chemicals used for lignin modification and bleaching of wood were sodium hydroxide (NaOH, 98.0%, Samchun Pure Chemical, South Korea), sodium sulfite (Na_2SO_3, Daejung Chemicals, South Korea), and hydrogen peroxide (H_2O_2, 30%, Daejung Chemicals, South Korea). UV-curing polymer (NOA 63, Norland Products, USA) and epoxy resin (bisphenol A and triethylenetetramine, R&B, South Korea) were used as the infiltration polymers. 8CB was supplied by Tokyo chemical Industry, Japan.

Lignin modification and bleaching of wood NWs were dried in an oven at 150 °C before chemical processing. Solution containing 2.5 M NaOH and 0.4 M Na_2SO_3 in deionized (DI) water was utilized as the lignin modification solution. Wood slices were immersed in the lignin modification solution and allowed to boil for 6 h. Subsequently, the modified woods were immersed in a H_2O_2 (15 wt% in DI water) solution and allowed to boil for 1 h. When the samples turned visibly white, BWs were rinsed several times with ethanol followed by storage in acetone overnight until further use.

Fabrication of TWs and PDLC/TWs NOA 63 was chosen as the infiltration polymer for preparing TWs. BWs were infiltrated with NOA 63 solution overnight at 70 °C. Thereafter, the infiltrated woods were sandwiched between glass slides followed by curing for 30 min under UV light (4 W, 350 μW cm^{-2} at 15 cm) of 365 nm (TN-4LC, Korea Ace scientific, South Korea). After the completion of UV illumination, TWs were carefully peeled off from the glass slides. For comparison, two components, namely epoxy resin (bisphenol A) and a hardener (triethylenetetramine), were premixed at a ratio of 2:1. BWs were immersed in epoxy resin followed by infiltration under vacuum for 1 h. Woods synthesized using epoxy resin were cured in an oven at 70 °C for 4 h.

Herein, thermochromic PDLC/TWs were fabricated by introducing a mixture of LC (8CB) and NOA 63 into BWs. 8CB (30 vol%) were uniformly dispersed and mixed with the NOA 63 solution with a stirrer at 70 °C. Subsequently, BWs ($20\times20\times2$ mm^3) were immersed in the mixture (100 mL) overnight at 70 °C. Then, the infiltrated wood was sandwiched between glass slides followed by curing for 30 min under UV light (4W, 350 μW cm^{-2} at 15 cm) of 365 nm (TN-4LC, Korea Ace scientific, South Korea). After the completion of UV illumination, PDLC/TWs were carefully peeled off from the glass slides.

Characterizations Weight losses of lignin modified woods and BWs was calculated by Eq. 1:

$$\text{Weight loss} = \text{Original lignin content of the wood} - (M - m)/M \times 100\% \quad (1)$$

where M is original weight of woods, and m is weight after lignin modification or bleaching process. In this work, we used the original lignin values of 23.5, 22.5, and 32.5% for balsa, bass, and pine woods, respectively [38]. All samples were oven-dried at 70 °C for 24 h after chemical processing. Surface and cross-sections of the wood samples were analyzed using a scanning electron microscope (SEM, Tescan, MIRA3-LMH) operating at an acceleration voltage of 10 kV and energy-dispersive spectroscopy elemental maps. Cross-sections of the wood samples were prepared by fracturing TWs after freezing in the liquid N_2. Crystallinities of NWs and BWs were investigated by the X-ray diffraction (XRD, Rigaku, MiniFlex600, Cu Kα, λ = 1.54 Å). Crystallinity index (CI) values were estimated using the (002) main peak and amorphous fraction at 18°, according to the Segal method [42].

$$CI\ (\%) = (I002 - Iam)/I002 \times 100\% \quad (2)$$

Fourier transform infrared (FTIR) spectra were obtained in the range of 600−4000 cm^{-1} at RT (PerkinElmer, Spectrum 100). Raman spectra were measured using a Raman microscope (Horiba, LabRAM HR UV/Vis/NIR) equipped with a 514 nm laser (He–Ar laser) as a light source. The total transmittance and haze of the samples were measured by a UV–vis-NIR spectrophotometer (Shimadzu, UV-3600) equipped with an integrating sphere. Each measurement was conducted at least three times per sample to ensure reproducibility. Tensile properties of the wood sample before and after infiltration were examined using a universal testing machine (Shimadzu, AG–X). Measurements were performed at least five times for each species. Stretching directions of TWs were parallel to the aligned cellulose, and stretching speed was 1 mm min^{-1}. Young's moduli of TWs (E_{TW}) were calculated by the rule-of-mixture model [43–45]. To evaluate the E_{TW} in one direction, we speculated that both the polymer matrix and wood underwent the same strain, perfectly aligned parallel to the applied stress. This strain results from uniform stress applied across a homogeneous cross-sectional area. Typically, the modulus is regarded as a linear function of the volume fraction. However, the same relationship also applies to the weight fraction. Rule-of-mixture equation (Eq. 3) for calculating the E_{TW} in the wood direction was derived from the Young's moduli of the two elements [43–45].

$$E_{TW} = E_{wood}M_{wood} + E_{polymer}M_{polymer} \quad (3)$$

where E_{wood} and $E_{polymer}$ and M_{wood} and $M_{polymer}$ represent the experimental Young's moduli and weight percent of the wood and infilled polymer matrix, respectively.

Thermal conductivities of samples were measured using a thermal diffusivity measuring system (NETZSCH, LFA467). For each material, measurements were repeated five times to ensure reliability. Differential scanning calorimetry (DSC, Perkinelmer, DSC 8000) was conducted at a rate a 10 °C min^{-1} in a temperature range of 20–50 °C under a single pass of air flow. UV-blocking performances of the samples were characterized using a compact 365 nm UV lamp with a power of 4 W. UV lamp directly illuminated the samples on the top surface of the showcase ($7\times7\times7$ cm^3), and thereafter, the transmitted UV light illuminated the color-changeable sunglass. To investigate the heat conservation abilities of samples, we constructed house-like structures with windows of glass and PDLC/TW. Before the thermal experiment, an Al block as a heating block was heated in an oven at 150 °C for 3 h. Then, thermal changes of the model houses were examined by a thermal imaging camera for 60 min after placing the heated block inside the houses. All experiments were conducted in accordance

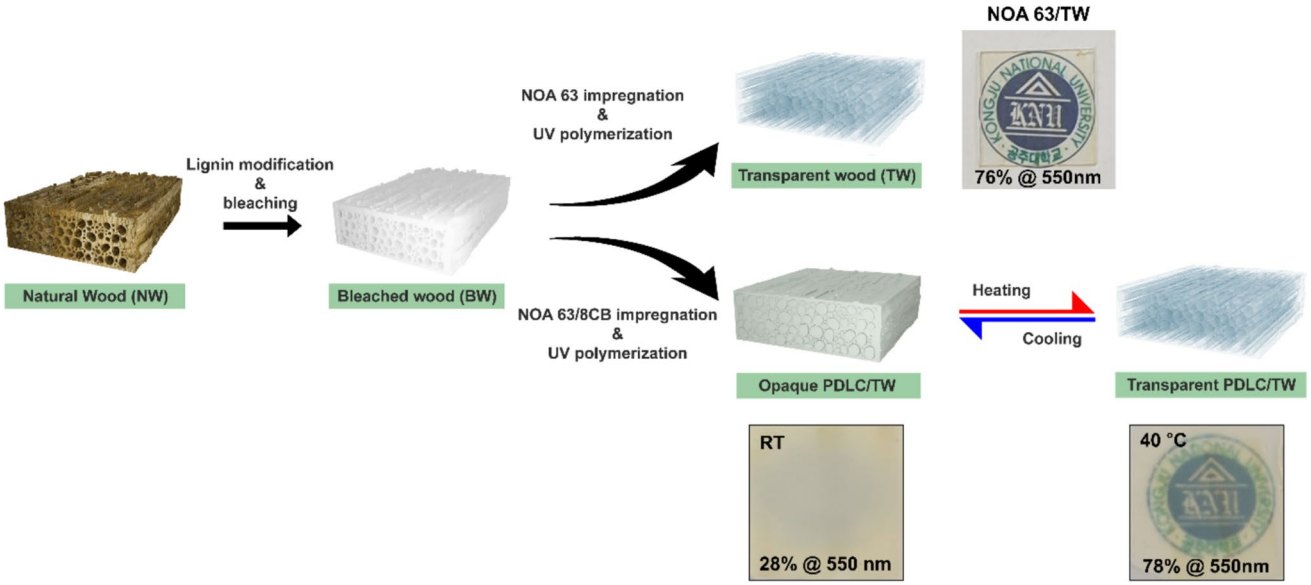


Fig. 2 Schematic of the preparation of NOA 63/TW and thermochromic PDLC/TW. Top right: image of NOA 63/TW placed on the surface of university logo with high transparency. Down: images of PDLC/TW at room temperature and 40 °C, exhibiting thermal switching of PDLC/TW between opaque and transparent phases

with applicable laws and received approval from the Institutional Review Board (IRB) at Kongju National University (KNU-IRB-2024–123). Informed and voluntary consent was obtained from the human participant involved in the experiments.

3 Results and discussion

NW appears opaque in visible light because of light scattering and reflection at the boundaries of cell walls and lumens, along with significant light absorption by light-absorbing components [37, 46]. To prepare TW, eliminating most of the light-absorbing materials or chromophoric components in the lignin is essential. NWs were initially treated with NaOH and Na_2SO_3 to modify lignin followed by bleaching with H_2O_2 (Fig. 2). Subsequently, BWs were separately impregnated with NOA 63 and PDLC (mixture of 8CB and NOA 63) followed by polymerization using UV light to fabricate TWs impregnated with NOA 63 (NOA 63/TWs) and PDLC/TWs, respectively. As depicted in the top-right image of Fig. 2, the mark beneath NOA 63/TW is clearly visible under ambient light. Notably, the optical properties of PDLC/TW could be precisely adjusted in accordance with the temperature (lower images of Fig. 2). Below RT, PDLC/TW demonstrates an opaque phase. However, when the temperature reaches 40 °C, PDLC/TW turns transparent, and therefore, the background is readable.

Due to their varying densities and lignin contents, three distinct types of woods (that is balsa, bass and pine) were chosen as the raw materials. Pine wood is generally denser than both balsa and bass woods and contains higher lignin contents as compared to those in balsa and bass woods. Li et. al have reported that the lignin contents of balsa, bass, and pine woods are 23.5, 22.5, and 32.5 wt%, respectively [38]. Fig. S1a–c show the weight loss of each type of wood as a function of lignin modification time from 1 to 9 h. For balsa, the majority of weight loss (9.40 wt%) occurred within the first hour. Then, the weight loss increased to 9.44, 11.56, 12.52, and 14.22 wt% after 2, 3, 6, and 9 h of treatment, respectively. In the case of bass wood, the weight losses were 5.92, 7.15, 10.77, 10.46, and 13.31 wt% for each lignin modification time. Additionally, pine wood exhibited weight losses of 3.08, 4.16, 5.53, 6.71, and 9.87 wt% at the corresponding lignin modification times. Overall, substantial weight loss occurred within 3 h of lignin modification, followed by a gradual increase in weight loss. Nevertheless, the weight loss nearly plateaued after 6 h of lignin modification, which was determined to be the optimal lignin modification time. After additional H_2O_2 bleaching, the final weight losses of balsa, bass and pine woods increased to 22.92, 22.09, and 20.51 wt%, respectively. Interestingly, although pine wood comprises the highest lignin content, it demonstrates the lowest weight loss when compared with the cases of balsa and bass woods. This indicates less delignification of pine wood during lignin modification and bleaching.

Figure 3a shows SEM images of balsa NW and final BW. Natural balsa wood exhibits a brown color; however, the

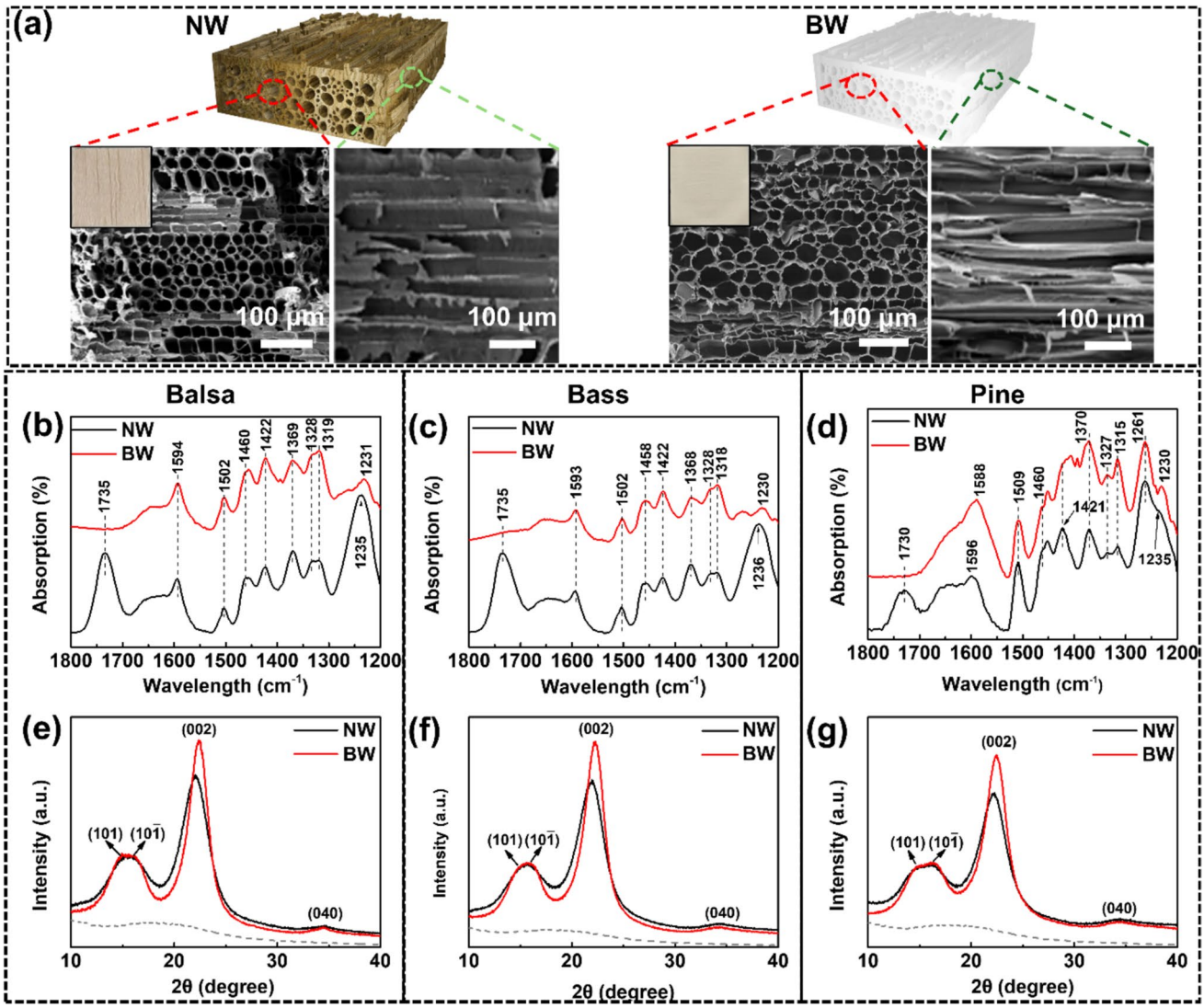


Fig. 3 **a** SEM images of the transverse and longitudinal sections of balsa NW and balsa BW (Inset: images of balsa NW and BW, respectively). FTIR spectra of (**b**) balsa, **c** bass, and (**d**) pine NWs and BWs. XRD patterns of **e** balsa, **f** bass, and (**g**) pine NWs and BWs

sample turned white after lignin modification and bleaching (Fig. 3a inset). Clearly, the hollow structure of the wood was effectively maintained after lignin modification and bleaching, providing an efficient pathway for subsequent infiltration of the polymer. Interestingly, the pore sizes of the balsa and bass woods slightly increased and cell walls became slightly thinner after lignin modification and bleaching (Fig. 3a and S2). Nevertheless, the pore size of pine did not change owing to the dense structure of this wood. FTIR spectra of balsa, bass, and pine NWs and corresponding BWs were depicted in Fig. 3b, c, and d, respectively. In the FTIR spectra of balsa NW and BW, the relative intensities of the bands corresponding to aromatic skeleton vibrations in lignin, located around 1594, 1502, 1460, and 1422 cm^{-1}, are quite similar. No significant decrease in intensity is observed, which conforms that the main aromatic part of lignin is substantially preserved in the wood structure after lignin modification and bleaching [38, 47, 48]. Relative bands corresponding to aromatic skeleton vibrations are also present in the FTIR spectra of bass and pine BWs, indicating retention of the lignin structure. However, the peak at 1735/1730 cm^{-1} related to C=O stretching in hemicellulose is absent in the spectra of all BWs, and the intensity of the peak around 1369 cm^{-1} associated with C−H deformation in cellulose and hemicellulose is low as compared to the case before bleaching [30]. Moreover, the intensity of the peak around 1235 cm^{-1} corresponding to syringyl ring and C−O stretching in lignin and hemicellulose considerably decreased after bleaching [30]. This suggests partial degradation of lignin and hemicellulose during lignin modification and bleaching. XRD patterns of the cellulose crystal structure in both NWs and final BWs were also analyzed (Fig. 3e–g). Diffraction peaks

around 16 and 22° are detected for all samples, attributed to the (101) and (002) cellulose crystal planes, verifying that lignin modification and bleaching did not alter the crystal structures of the woods. Furthermore, the relative CI plays a crucial role in determining the mechanical and thermal properties of woods. CI values of balsa, bass, and pine BWs are 76.8, 77.3, and 71.6%, respectively, which are higher than those of balsa (64.4%), bass (64.4%), and pine (61.0%) NWs, respectively. Increase in CI is clearly caused by the partial removal of lignin and hemicellulose. Nevertheless, CI enhancement in the case of pine wood (10.6%) is less than that in the cases of balsa (12.4%) and bass woods (12.9%), implying the removal of smaller amounts of lignin from pine wood, which is consistent with the observed weight loss. Consequently, after polymer infiltration, pine wood demonstrated a yellow color as compare to the case of balsa and bass woods, due to the relatively higher lignin contents remained in the wood (inserts of Fig. 4a–c).

NOA 63 was selected as the polymer matrix, which is a thiol−ene-based photocurable polymer that can be cured in just minutes with UV light and exhibits high optical transparency across a wide spectral range [49–51]. Quick curing of NOA 63 using low-intensity UV light provides a significant advantage over traditional epoxy-based embedding resins using heat curing, specifically for rapid prototyping. Furthermore, the refractive index of NOA 63 is approximately 1.56, which matches that of wood (cellulose (1.53), hemicellulose (1.53), and lignin (1.61)) [28, 32, 41, 49]. Woods became transparent after infiltration and UV curing with NOA 63 (insets of Fig. 4a–c). University logo beneath TW is clearly visible, demonstrating excellent transparencies of the as-synthesized woods. In contrast, the original woods exhibited transmittance close to 1%, indicating that they were opaque. Moreover, the transmittances for balsa, bass, and pine NOA 63/TWs reached 76, 76, and 64% at a wavelength of 550 nm, respectively. Transmittances for balsa, bass, and pine TWs filled with epoxy resin (Epoxy/TWs) were 56, 70, and 44% at 550 nm, respectively. SEM images (Fig. 4a–c) reveal that the NOA 63 can indeed completely fill the voids and cell walls of the woods and frameworks of the NW microstructures remain intact after polymer infiltration and photopolymerization of NOA 63. Additionally, the bond between NOA 63 and the cell wall is well-defined, and no noticeable gaps or boundaries are observed (Fig. 4d and S3). However, cracks or gaps appeared along the interface between the epoxy polymer and cell wall owing to shrinkage of the epoxy resin during curing (Fig. 4e and S4) [28, 31, 34, 36]. Consequently, light scattering was enhanced, and the

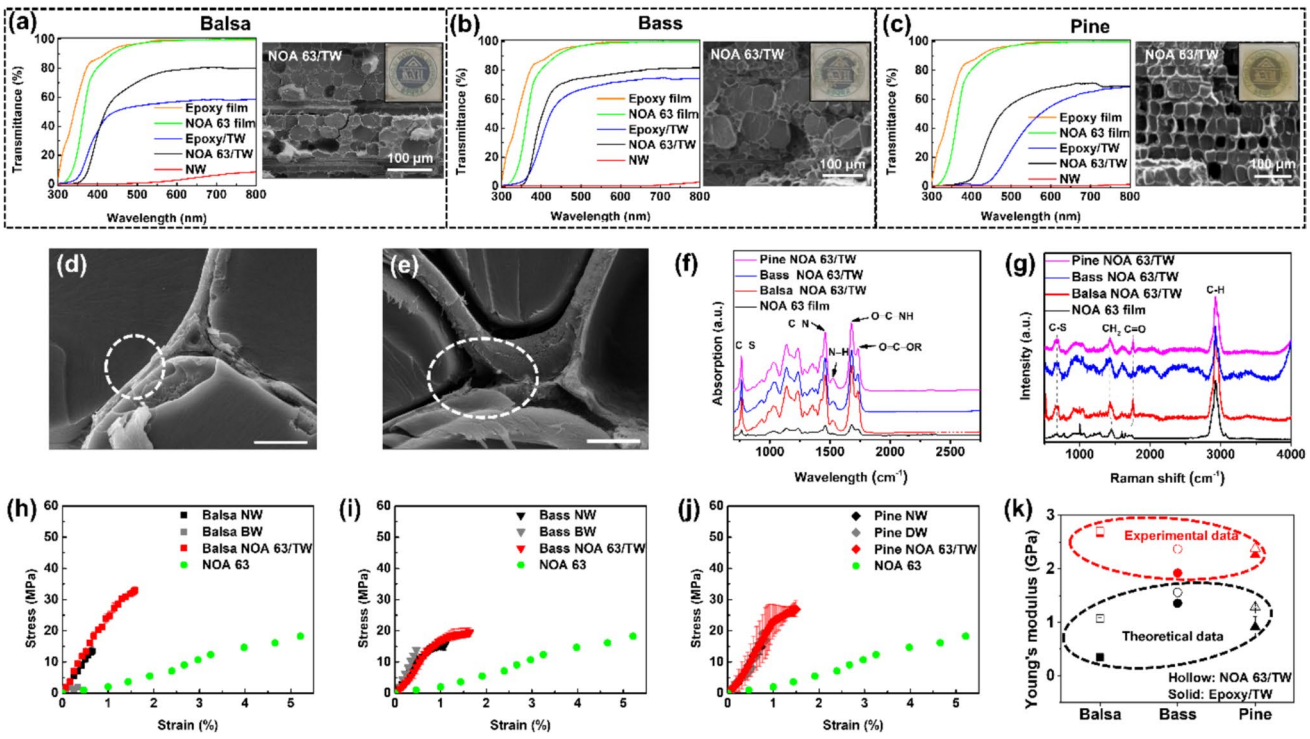


Fig. 4 **a–c** Transmittance spectra of as-prepared balsa, bass, and pine TW with different infilled polymers and SEM images of NOA 63/TWs. Insets in SEM images: images of NOA 63/TWs. **d** High-magnification SEM images of balsa NOA 63/TW. **e** High-magnification SEM images of balsa Epoxy/TW. **f** FTIR and (**g**) Raman spectra of as-prepared NOA 63/TWs with various wood species. **h–j** Experimental stress–strain curves of NOA 63, NWs, BWs, and NOA 63/TWs fabricated using (**h**) balsa, **i** bass, and (**j**) pine woods. **k** Comparison of experimental and theoretical Young's moduli

woods filled with epoxy resin demonstrated lower optical transmittances than those of corresponding NOA 63/TWs. Furthermore, to improve the optical transparency of TW composites, it is essential to reduce the refractive index difference between the wood template and the infiltrating polymer. A larger mismatch in refractive indices typically results in increased light scattering, thereby decreasing transmittance. Epoxy resin, with a refractive index of approximately 1.5, exhibits a larger mismatch with wood cell wall (~ 1.56) compared to NOA 63 (~ 1.56), making NOA 63 more suitable for achieving enhanced optical transparency in TW composites [5, 28]. Ultimately, high transparency of NOA 63/TW can be attributed to well-matched refractive index of NOA 63 with that of the wood, along with a uniform interface between the polymer and cell walls.

NOA 63-infiltrated TWs were also investigated by FTIR and Raman spectroscopies (Fig. 4f and g). NOA 63 consists of 1,3,5-triallyl-1,3,5-triazine-2,4,6(1H,3H,5H)-trione (TATATO) and acrylate (OCO−CH═CH_2) monomer units with mercaptoester (OCO−S−H) groups [52]. Thiol−ene photopolymerization follows a stepwise growth mechanism involving a combination of C═C bonds and thiol groups (−SH) [41, 50, 53]. FTIR spectrum of the NOA 63 film exhibits two amide (−CONH−) bands at 1681 and 1519 cm^{-1} ascribed to TATATO in the polymer matrix (Fig. 4f). First amide band, associated with carbonyl stretching (HN−C═O), slightly shifted to 1679 cm^{-1} for all three TWs. Second amide band, related to the N−H bending vibration, slightly shifted to 1521, 1525, and 1524 cm^{-1} for balsa, bass, and pine TWs, respectively. Peaks shift and their intensities increased upon the incorporation of NOA 63 into the wood, indicating an interaction between the wood and polymer and a homogeneous distribution of the polymer in the wood [49]. Furthermore, the peaks corresponding to the C−S stretching vibration, C−N stretching vibration, and ester carbonyl stretching are detected at 765, 1460, and 1732 cm^{-1}, respectively. Interestingly, after polymer infiltration, the peaks at 1732 cm^{-1}, which had disappeared after lignin modification and bleaching, reappeared. Moreover, the peaks attributed to the S−H band around 2550 cm^{-1} are not noticed for all three TWs, which confirms appropriate infiltration of NOA 63 polymer in the wood by the thiol−ene reaction [49]. Raman spectra of all the samples demonstrate the most prominent and characteristic features: the C−S band at 673 cm^{-1}, CH_2 bending in the region between 1400 and 1500 cm^{-1}, and C−H stretching in the range of 2900–3100 cm^{-1} (Fig. 4g). Among them, the CH_2 bending peak shifted from 1449 cm^{-1} to 1429 cm^{-1} when NOA 63 was infilled in TWs. Additionally, the peak for ester carbonyl stretching (R−C═O−O−R') appeared at 1735 cm^{-1} in the spectrum of the NOA 63 film [53]. Moreover, the intensities of these ester carbonyl stretching peaks were significantly high and these peaks slightly shift to 1755, 1758, and 1756 cm^{-1} for balsa, bass, and pine TWs, respectively. Similar to the cases of FTIR spectra, the shifts in the peaks and high peak intensities suggest interaction of the polymer with wood and adequate distribution of the polymer in the wood. Overall, NOA 63 forms homogeneous polymer networks inside the wood and can be prepared in minutes via photopolymerization, which allows rapid prototyping of TW.

To evaluate the potential of TW for window applications, the mechanical properties of the prepared TW samples were analyzed, and the corresponding stress–strain relationships are shown in Fig. 4 h–k and S5. Compared with the cases of NWs, the tensile stress of each TW increased after polymer infiltration. Tensile stresses of balsa, bass, and pine woods increased from 13.48, 15.57 and 14.91 MPa to 32.96, 19.43, and 26.92 MPa, respectively, after the injection of NOA 63 into the woods. In addition to reducing the light scattering, NOA 63 can improve the mechanical strength of TW when compared with those of NW substrates owing to the synergy between wood and NOA 63. Interestingly, although balsa NW was the weakest wood among the three woods, the polymer-infiltrated balsa wood exhibited the highest mechanical property due to polymer infiltration into larger pores of the wood channels and additional pores on the cell walls [37]. Moreover, after injecting epoxy resin, the tensile stresses of balsa, bass, and pine TWs were increased to 50.54, 25.93, and 30.10 MPa, respectively, which are higher than that of NOA 63/TW. This is ascribed to the higher tensile stress of the raw epoxy resin than that of raw NOA 63 (Fig. S5). Based on the strain and stress data, the E_{TW} was calculated using the rule-of-mixtures model [43–45]. E_{TW} values for balsa, bass, and pine NOA 63/TWs are 1.07, 1.56, and 1.28 GPa, respectively (Fig. 4k), which are higher than those of Epoxy/TW. However, the experimental Young's moduli for balsa, bass, and pine NOA 63/TWs are 2.7, 2.37, and 2.38 GPa, respectively, which are 52–152% higher than the theoretical values for NOA 63/TW and even comparable to the experimental values for Epoxy/TWs. This implies that NOA 63 not only fills the pore structures of TW, but also enhances the elastic properties of TW.

Although as-synthesized TWs demonstrated better optical and mechanical properties than those of NWs, they lacked the abilities to control their optical properties for smart window applications. For smart window applications, thermochromic PDLCs are attractive materials that can regulate transparency via temperature without power supply. In most studies the PDLC solutions were coated on the glass or transparent electrode for smart window applications [15, 16, 19, 21, 54]. Herein, we controlled the transparency directly using as-prepared PDLC/TW. Among the many LCs, we chose 8CB because its refractive index is most similar to those of cellulose and NOA 63, and most importantly, its transparency can be regulated by temperature. Balsa, bass, and pine PDLC/TWs were opaque at temperatures

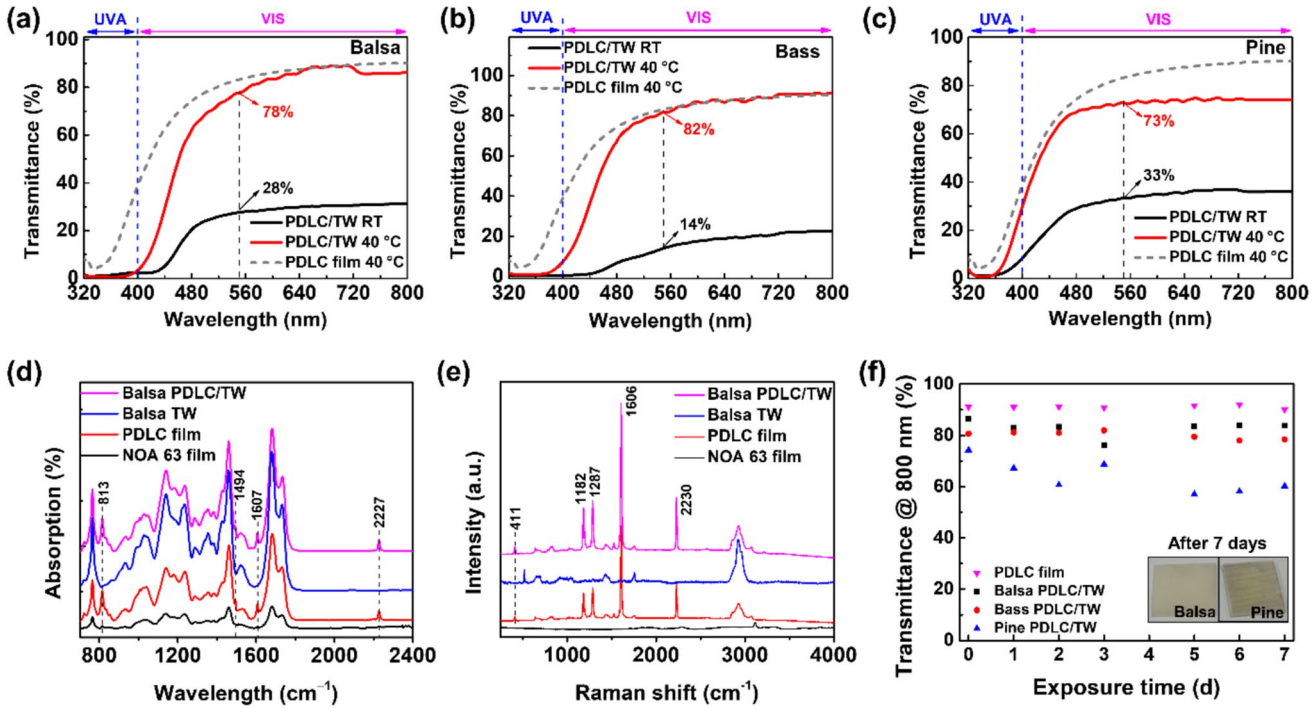


Fig. 5 **a–c** Optical transmittance spectra of (**a**) balsa PDLC/TW, **b** bass PDLC/TW, and (**c**) pine PDLC/TW. **d** FTIR and (**e**) Raman spectra of the pure NOA 63 film, PDLC film, balsa NOA 63/TW, and balsa PDLC/TW. **f** Variations in the optical transmittances of PDLC film and PDLC/TWs at 800 nm under UV treatment. Insets: images of balsa and pine PDLC/TWs after 7 days of UV treatment

below 25 °C and became transparent when the temperature exceeded 40 °C (Fig. 2 and S6). PDLC/TWs exhibited high transparencies above 40 °C, and the university logo beneath them was clearly visible. SEM images of the surfaces of PDLC/TWs are depicted in Fig. S6, demonstrating complete infiltration of PDLCs into the hollow wood channels. Presence of LCs did not impact the compatibility between the injected polymer and wood. At RT, the transmittances of balsa, bass, and pine PDLC/TWs were 28, 14, and 33% at a wavelength of 550 nm, respectively (Fig. 5a–c). In contrast, at 40 °C, the transmittances of balsa, bass, and pine PDLC/TWs increased to 78, 82, and 73% at the same wavelength of 550 nm, respectively. The haze values of PDLC/TWs prepared from balsa, bass, and pine were measured to be 57, 88, and 92% at a wavelength of 550 nm, respectively (Fig. S7). Although infiltration with NOA 63 and LC droplets aims to minimize refractive index mismatches, the intrinsic porous structure and anisotropic cellular arrangement of the wood substrate inherently promote light scattering. Currently, haze values of TW commonly range from 40 to over 90% [28]. Achieving an optimal balance between high optical transmittance and low haze remains a significant challenge in the development of sustainable wood-based transparent materials. It is strongly influenced by factors such as wood species, structural density, infiltration polymer and processing conditions. Only a few studies have reported TW with low haze values. For instance, Jia et al. [55] achieved a haze of 10% in 0.7 mm thick TW using a strong hydrolysis treatment to remove light-scattering components. However, haze is highly thickness-dependent; the same TW exhibited a haze of approximately 40% at 1.5 mm thickness. This increase is attributed to a longer pathway and a higher number of polymer/wood interfaces, which enhance light scattering. In another study, Höglund et al. [53] obtained similarly low haze (10%) in 1.2 mm thick TW through a bleached process that selectively removed chromophores while retaining most lignin and hemicellulose. However, a delignified wood template of the same thickness (1.2 mm) exhibited a much higher haze of 63%, suggesting that the degree of lignin removal may also play a critical role in determining the optical haze of TW. In addition, the effect of sample thickness on the thermochromic behavior of balsa PDLC/TW was examined by comparing specimens with thickness of 1 mm and 2 mm (Fig. S8 and 5a). At 40 °C, both samples exhibited similar optical transmittance at 550 nm. However, at RT, the 1 mm sample showed slightly higher transmittance than the 2 mm sample. Although previous studies have reported that decreasing thickness can decrease haze, our results indicate that the variation in thermochromic performance diminishes as the thickness decreases. Consequently, a 2 mm thickness is considered more favorable, as it provides a larger

transmittance contrast during thermal switching, which is beneficial for smart window applications.

Interestingly, PDLC/TWs exhibited excellent UV-blocking performances. At RT, opaque balsa and bass PDLC/TWs effectively blocked almost 100% of the ultraviolet A (UVA) radiation (320–400 nm), which represents the majority of the UV radiation that reaches the Earth's surface. Additionally, transparent balsa and bass PDLC/TWs at 40 °C effectively shielded most of the UVA radiation. Regrettably, the PDLC/TWs exhibit no significant variation in the near-infrared region between RT and 40 °C. Synergistic effect of PDLC and wood is particularly attractive and raises interesting questions. Comparing of the FTIR spectra of TWs and PDLC/TWs indicates new peaks corresponding to CN stretch at 2227 cm^{-1}, aromatic ring C=C stretch at 1607 and 1494 cm^{-1}, and aromatic C−H out-of-plane bending at 813 cm^{-1} in the spectra of PDLC/TWs (Fig. 5d and S9a and b) [56]. These peaks can be distinctly attributed to 8CB in NOA 63. In the Raman spectra of PDLC/TWs, new peaks corresponding to 8CB can also be identified (Fig. 5e and S9c). Peaks at 411 and 2230 cm^{-1} are ascribed to the C_{arom}−C≡N out-of-plane symmetric bending and C≡N stretching, respectively. Higher-intensity Raman bands are linked to aromatic ring deformations: the band at 1606 cm^{-1} is assigned to C−C aromatic ring breathing, the band at 1287 cm^{-1} is attributed to C−C biphenyl linking stretching, and the band at 1182 cm^{-1} is related to C−H in-plane deformation [57, 58]. Raw PDLC film demonstrated minimal UV absorbance in the UVA region; contrarily, balsa and bass PDLC/TWs exhibited strong UV absorbances (Fig. 5a). Red-shift of the UV absorbance indicates J-aggregation between 8CB and modified lignin in balsa and bass woods, which reduces the energy gap required for UV absorption, thereby increasing UV absorption [59, 60]. In contrast, the UV absorbance of pine PDLC/TW was lower. As mentioned earlier, the CI enhancement for pine wood was lower than those for balsa and bass woods, confirming the retention of high amounts of lignin in the pine wood after delignification and bleaching.

UV-blocking abilities of PDLC/TWs can effectively reduce the risks of damage to human skin, furniture, and interior displays from sunlight through windows. Moreover, UV stabilities of PDLC film and PDLC/TWs were assessed by exposing the samples to UV light for 7 days and measuring the transmittance at 800 nm (Fig. 5f). Compared to the cases of original PDLC film and PDLC/TWs, no significant degradation in the transmittances of PDLC film and balsa PDLC/TW were noticed. Transmittances of PDLC film, balsa and bass PDLC/TWs slightly decreased from 91, 86 and 81% to 90, 84 and 78% at 800 nm, respectively. However, transmittances of pine PDLC/TWs decreased from 74 to 60% at 800 nm owing to the partial degradation of lignin remaining in the wood. Residual lignin contained numerous chromophoric and auxochrome groups, which absorbed UV light and led to the aging and darkening of the PDLC/TW (Inset of Fig. 5f) [23, 48]. These results reveal short-term UV stabilities of balsa PDLC/TWs, highlighting their potentials for practical applications. Furthermore, the cycle stability of basla PDLC/TW was evaluated over 100 successive heating and cooling cycles, during which the material maintained relatively stable transmittance and good visible light modulation performance (Fig. S10).

As-prepared PDLC/TWs exhibited thermal switching from opaque to transparent phases. Reversible thermo-switching can be triggered by the phase transition temperatures, corresponding to three phases of 8CB: smectic A (SmeA), nematic (N), and isotropic (I) [56, 61]. Appropriate phase transition temperatures of 8CB in the PDLC film and PDLC/TW were determined using DSC (Fig. S11). Generally, with an increase in temperature, 8CB transforms from SmeA to the N and then to I. Phase transition temperatures of SmeA-N (T_{S-N}) and N-I (T_{N-I}) in the PDLC film were measured to be 31.4 and 37.8 °C, respectively. Interestingly, in addition to the SmeA-N transition temperature of 32.2 °C, PDLC/TWs demonstrate double N-I transition temperatures of 36.5 and 38.1 °C due to surface- and bulk-related N-I transitions, respectively [62]. When the temperature was increased from RT to 40 °C, as-fabricated PDLC/TW changed stepwise from the opaque phase to the translucent phase and finally reached the transparent phase (Fig. 6a-c inset). At RT, randomly oriented LCs (8CB) in SmeA are observed, and consequently, opaque PDLC/TW blocks the view (Fig. 6a). As shown in Fig. 6b, 8CB is at the turning point between SmeA and N with a randomly oriented structure, partially blocking the view (translucent state). At a high temperature (T > 40 °C), 8CB transforms from N to I, and PDLC/TW is transparent, where the background is clearly visible (Fig. 6c). As-synthesized PDLC/TWs exhibit thermal switching from the opaque to transparent phase via phase transition of LCs (Video S1). Below RT, SmeA of the LC molecules is randomly oriented in the polymer matrix, causing PDLC/TW to appear opaque owing to the refractive index mismatch between SmeA phase of 8CB (ordinary refractive index (n_o) ≈ 1.51 and extraordinary refractive index (n_e) ≈ 1.68) and NOA 63 (1.56) (Fig. 6d (i)) [63]. Anisotropic LC demonstrates two principal refractive indices: n_o and n_e, which represent the ordinary and extraordinary refractive indices of the LC in the ordinary and extraordinary modes, respectively. As the temperature rises, the liquid crystal undergoes a transition to the isotropic phase, eliminating the distinction between the ordinary and extraordinary refractive indices [63]. In the optically isotropic state, the refractive index of the liquid crystal droplets (n_{iso} = 1.56) matches that of NOA 63 (1.56), allowing light

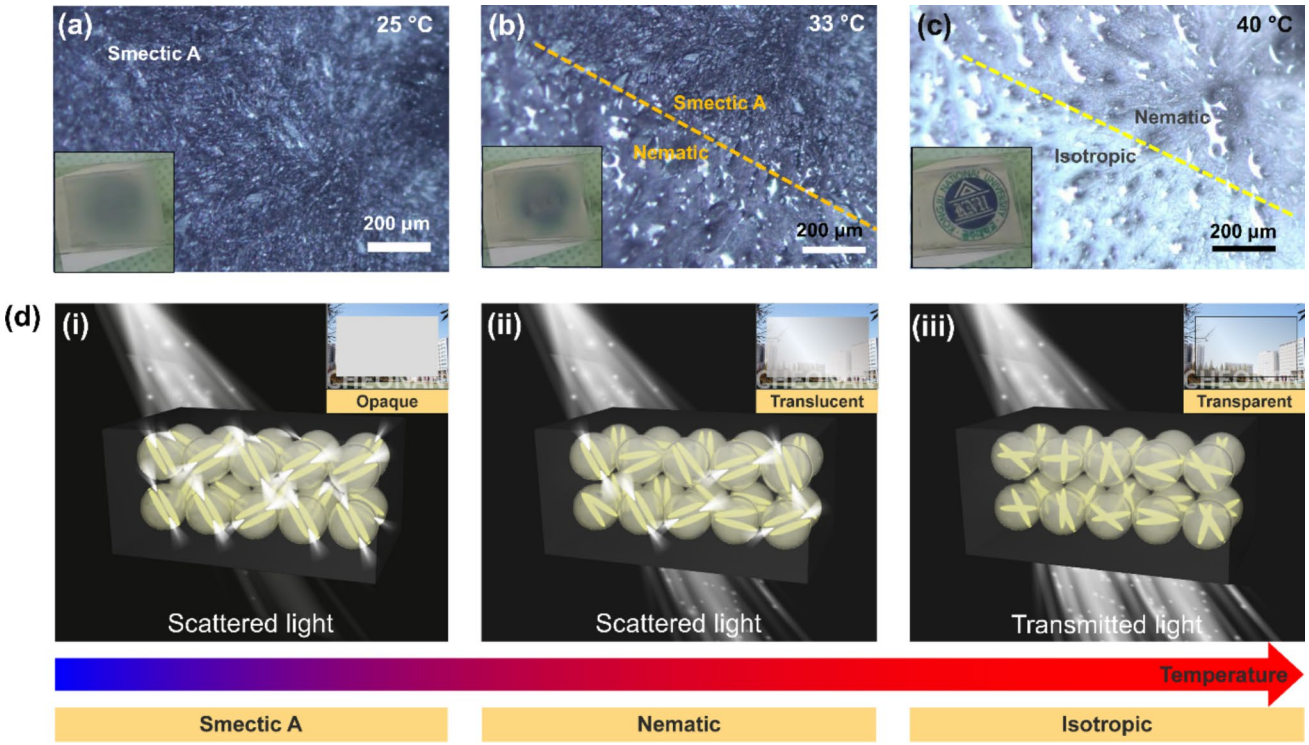


Fig. 6 **a**–**c** Optical microscopy images of the PDLC/TWs at different temperatures. Each set of images represents the same sample area. Image (**a**) is a microscopy image of the smectic A liquid crystal at 25 °C. Image (**b**) denotes a microscopy image of the liquid crystal phase change between smectic A and nematic at 33 °C. Image **c** represents a microscopy image of the liquid crystal phase change between nematic and isotropic at 40 °C. **d** Schematic of (i) smectic A of 8CB randomly aligned in PDLC/TW, resulting in an opaque state, (ii) nematic of 8CB randomly aligned in PDLC/TW, leading to a translucent state, and (iii) isotopic of 8CB in PDLC/TW, demonstrating transmission of light

to pass through with minimal scattering and yielding high optical transparency (Fig. 6d (iii)).

As-developed thermochromic PDLC/TWs exhibit potentials for application as building windows, replacing traditional glass windows, because of their environmental friendliness, transparency, and UV protection properties. Balsa PDLC/TW was selected as the representative functional component for possible application as an efficient smart window material due to its high transparency and UV protection properties. Briefly, a large PDLC/TW template ($7 \times 7 \times 0.2$ cm^3) was prepared as a window for one side of a showcase (Fig. 7a and b). Figure 7a shows real images of the PDLC/TW window in both transparent and opaque states in an outdoor setting. During the day, with an increase in the temperature, the PDLC/TW window becomes transparent, allowing sunlight to enter and enhance indoor lighting. At night, the PDLC/TW window can switch to opaque state, reducing visibility from outside and helping to maintain indoor privacy. However, at the current transition temperature of the PDLC/TW, the transition to the transparent state occurs under typical daytime conditions during the warm season. During the cold season, auxiliary systems such as heating films or responsive electrical control units are required to maintain reliable performance independent of ambient temperature. Additionally, upon being exposed to abundant sunlight, the PDLC/TW window will be subjected to UV rays. Therefore, UV-blocking properties of the samples were evaluated using a UVP compact UV lamp (4 W, 365 nm) as the light source. UV light was perpendicularly directed onto the sample from the upper side (sunroof) of the showcase and then onto the UV-sensitive color-changing sunglass inside the showcase (Fig. 7b). PDLC/TW sunroof demonstrated significantly better UV-blocking properties than those of the glass sunroof. For opaque PDLC/TW at 25 °C, the incoming UV light was blocked and absorbed by the PDLC/TW sunroof, maintaining the color of the sunglass. After 1 min of exposure to UV light, the sunglass exhibits a transmittance of 99.9% at 550 nm (Fig. S12). When PDLC/TW was heated to 40 °C, the transparent PDLC/TW sunroof continued to block UV light without affecting the color of the sunglass with a transmittance of 99.4% at 550 nm. In contrast, the glass sunroof allowed UV light to directly pass through it, rendering the sunglass to transform to dark black with a transmittance of 72.1% at 550 nm. These results suggested that the PDLC/TW

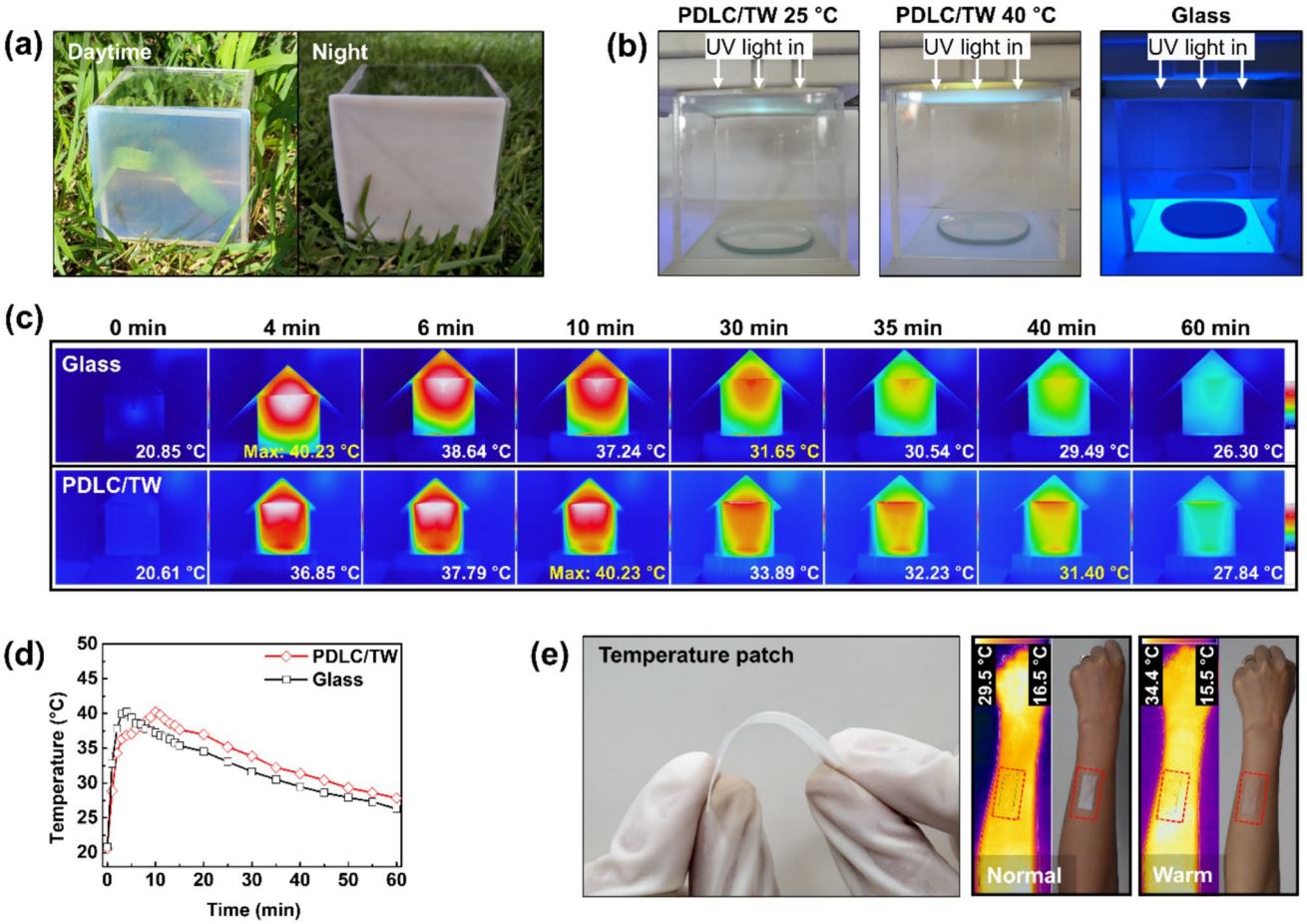


Fig. 7 **a** Images of PDLC/TW as one side of the showcase during the day and at night. **b** Images of PDLC/TW and glass as one side of the showcase under UV illumination. **c** Thermal images of glass and PDLC/TW model houses according to the time. **d** Time-dependent temperature changes inside the model house separately constructed using glass and PDLC/TW. **e** Images of the temperature patch for real-time body temperature check

selectively block UV light to shield humans and indoor furniture from UV damage. Moreover, considering the demand for energy-saving building materials, thermal conductivity is another important property for smart windows. Thermal insulation of windows is crucial because it facilitates slow transfer of heat through windows or roofs, rendering the house warmer in winter and cooler in summer. PDLC/TW exhibits a substantially lower thermal conductivity of 0.197 W m^{-1} K^{-1} as compared to that of glass (0.911 W m^{-1} K^{-1}) (Fig. S12), and thus, it is highly beneficial for thermal insulation and effectively reducing energy loss. Because of its combination of adjustable optical properties and low thermal conductivity, PDLC/TW demonstrates excellent potential as a transparent, energy-efficient smart window material that can replace glass. To assess the heat insulation performance of PDLC/TW, temperature variations were measured inside a model house where both the roof and windows were constructed using PDLC/TW. For comparison, a version of the model house developed using standard glass was also examined. We used Al blocks as the heating source. Time-dependent temperature changes for the samples are shown in Fig. 7c and d. Temperature of the model house constructed using glass rapidly increased from 20.85 to 40.23 °C, a considerable increase of 19.38 °C, after the heating blocks were placed inside this house for 4 min. In contrast, the temperature of the model house built using PDLC/TW increased from 20.61 to 40.23 °C in 10 min, which was a slower increase than the temperature increase observed for the glass house. Once the temperature peaked, it gradually began to decrease for the PDLC/TW house. Low thermal conductivity of PDLC/TW helps to regulate the heat inside the house by allowing the temperature to more slowly increase and decrease, which is beneficial for energy-efficient heating and cooling systems. As demonstrated, PDLC/TW can efficiently capture sunlight for indoor illumination, block UV light, and reduce heat transfer through windows, rendering it a viable alternative to conventional glass. In

addition to the window/roof application, PDLC/TW can be used in intelligent temperature-monitoring devices owing to the reversible transparent-to-opaque transitions within the human body temperature. To monitor human body temperature in real time, we prepared a PDLC/TW sheet with thickness of 0.257 mm, which was attached to a wearable skin patch as a wristband. PDLC/TW sheet was applied to the wrist of the volunteer (Fig. 7e). When the temperature exceeded 38 °C, the sheet changed from opaque to transparent, signaling an increase in body temperature and the need for a medical check-up. These results demonstrate significant potential of PDLC/TW with integrated advantageous optical, thermal and mechanical properties for use in sustainable, energy-efficient buildings and wearable temperature sensors.

4 Conclusion

In summary, herein, thermochromic TWs were successfully fabricated by incorporating refractive index-matching LC (8CB) and UV-curing polymer (NOA 63) into wood templates for use in smart windows. Synergy effects of PDLC and the modified wood provide PDLC/TW with adjustable visible transparency based on temperature, which is advantageous for daylighting and maintaining privacy at night. More importantly, balsa PDLC/TW demonstrate excellent UV-blocking and thermal-insulating properties, effectively shielding against UV light and retaining a comfortable indoor temperature. This helps protect the human skin, prevent the aging of household items, and lower energy consumption for indoor temperature regulation. These findings highlight the considerable potentials of PDLC/TWs for application in next-generation energy-efficient buildings.

Supplementary Information The online version contains supplementary material available at https://doi.org/10.1007/s42114-025-01481-0.

Author contribution The manuscript was written with contributions from all authors. The experiments were conceptualized by Jin Kim, Dong Ju Lee and Sung Ho Song. The conduction of experiments and organization of data were performed by Cheng Ai Li, Jae Gyu Ahn, Hyeon Ji Jeong, Jang Hee Kim, Taeyoung Park and Do Kyoung Han. All authors contributed to the data analysis and discussion of the results. All authors have read and agreed to the published version of the manuscript.

Funding This research was supported by Basic Science Research Program through the National Research Foundation of Korea funded by the Ministry of Education (RS-2019-NR040074). This work was supported by the National Research Foundation of Korea (NRF) grant funded by the Korea government (MSIT) (RS-2025–00558261) and IITP (Institute of Information & Communications Technology Planning & Evaluation)-ITRC (Information Technology Research Center) (IITP-2025-RS-2024–00438335, 25%) grant funded by the Korea government(Ministry of Science and ICT). This research was supported by Korea Basic Science Institute (National Research Facilities and Equipment Center) grant funded by the Ministry of Education. (RS-2022-NF000835).

Data availability No datasets were generated or analyzed during the current study.

Declarations

Competing interests The authors declare no competing interests.

Open Access This article is licensed under a Creative Commons Attribution-NonCommercial-NoDerivatives 4.0 International License, which permits any non-commercial use, sharing, distribution and reproduction in any medium or format, as long as you give appropriate credit to the original author(s) and the source, provide a link to the Creative Commons licence, and indicate if you modified the licensed material. You do not have permission under this licence to share adapted material derived from this article or parts of it. The images or other third party material in this article are included in the article's Creative Commons licence, unless indicated otherwise in a credit line to the material. If material is not included in the article's Creative Commons licence and your intended use is not permitted by statutory regulation or exceeds the permitted use, you will need to obtain permission directly from the copyright holder. To view a copy of this licence, visit http://creativecommons.org/licenses/by-nc-nd/4.0/.

References

1. Yang Y, Liu X, Wan C, Liu S, Li X, Zhu Y, Yang Z, Li L, Zhang Z, Zhou Z, Xie Y, Zhao X, Chai H, Wu Y (2024) Powering the future green buildings: multifunctional ultraviolet-shielding transparent wood. ACS Nano 18(32):21288–21301. https://doi.org/10.1021/acsnano.4c05151
2. Mi R, Chen C, Keplinger T, Pei Y, He S, Liu D, Li J, Dai J, Hitz E, Yang B, Burgert I, Hu L (2020) Scalable aesthetic transparent wood for energy efficient buildings. Nat Commun 11(1):3836. https://doi.org/10.1038/s41467-020-17513-w
3. Ding Y, Pang Z, Lan K, Yao Y, Panzarasa G, Xu L, Lo Ricco M, Rammer DR, Zhu J, Hu M, Pan X, Li T, Burgert I, Hu L (2022) Emerging engineered wood for building applications. Chem Rev 123(5):1843–1888. https://doi.org/10.1021/acs.chemrev.2c00450
4. Xu G, Xia H, Chen P, She W, Zhang H, Ma J, Ruan Q, Zhang W, Sun Z (2022) Thermochromic hydrogels with dynamic solar modulation and regulatable critical response temperature for energy-saving smart windows. Adv Funct Mater 32(5):2109597. https://doi.org/10.1002/adfm.202109597
5. Zhang L, Wang A, Zhu T, Chen Z, Wu Y, Gao Y (2020) Transparent wood composites fabricated by impregnation of epoxy resin and W-doped VO_2 nanoparticles for application in energy-saving windows. ACS Appl Mater Interfaces 12(31):34777–34783. https://doi.org/10.1021/acsami.0c06494
6. Du Y, Liu S, Li Y, Chen X, Ho TC, Chao LC, Tso CY (2023) Perovskite-coated thermochromic transparent wood: a novel material for smart windows in energy-efficient and sustainable buildings. ACS Appl Mater Interfaces 15(42):49665–49677. https://doi.org/10.1021/acsami.3c11706
7. Tan S, Guo S, Wu Y, Zhang T, Tang J, Ji G (2024) Achieving broadband microwave shielding, thermal management, and smart window in energy-efficient buildings. Adv Funct Mater. https://doi.org/10.1002/adfm.202415921

8. Godar DE (2005) UV doses worldwide. Photochem Photobiol 81(4):736–749. https://doi.org/10.1111/j.1751-1097.2005.tb01438.x
9. Jansen R, Wang SQ, Burnett M, Osterwalder U, Lim HW (2013) Photoprotection: part I. Photoprotection by naturally occurring, physical, and systemic agents. J Am Acad Dermatol 69(6):853.e1-853.e12. https://doi.org/10.1016/j.jaad.2013.08.021
10. Lopez J, Sain M, Cooper P (2006) Performance of natural-fiber-plastic composites under stress for outdoor applications: effect of moisture, temperature, and ultraviolet light exposure. J Appl Polym Sci 99(5):2570–2577. https://doi.org/10.1002/app.22884
11. Wang JL, Sheng SZ, He Z, Wang R, Pan Z, Zhao HY, Liu JW, Yu SH (2021) Self-powered flexible electrochromic smart window. Nano Lett 21(23):9976–9982. https://doi.org/10.1021/acs.nanolett.1c03438
12. Yu Z, Yang Y, Shen C, Mao L, Cui C, Chen Z, Zhang Y (2023) Thermochromic hydrogels with an adjustable critical response temperature for temperature monitoring and smart windows. J Mater Chem C 11(2):583–592. https://doi.org/10.1039/D2TC04347E
13. Li K, Meng S, Xia S, Ren X, Gao G (2020) Durable and controllable smart windows based on thermochromic hydrogels. ACS Appl Mater Interfaces 12(37):42193–42201. https://doi.org/10.1021/acsami.0c12710
14. Wang D, Chen G, Fu J (2024) Multifunctional thermochromic smart windows for building energy saving. J Mater Chem A 12:12960–12982. https://doi.org/10.1039/D4TA01767F
15. Guo SM, Liang X, Zhang CH, Chen M, Shen C, Zhang LY, Yuan X, He BF, Yang H (2017) Preparation of a thermally light-transmittance-controllable film from a coexistent system of polymer-dispersed and polymer-stabilized liquid crystals. ACS Appl Mater Interfaces 9(3):2942–2947. https://doi.org/10.1021/acsami.6b13366
16. Kakiuchida H, Matsuyama A, Ogiwara A (2019) Normal-and reverse-mode thermoresponsive controllability in optical attenuation of polymer network liquid crystals. ACS Appl Mater Interfaces 11(21):19404–19412. https://doi.org/10.1021/acsami.9b01280
17. Shen W, Li G (2023) Recent progress in liquid crystal-based smart windows: materials, structures, and design. Laser Photon Rev 17(1):2200207. https://doi.org/10.1002/lpor.202200207
18. Wang X, Hu W, Chen H, Saeed MH, Huang J, Hu J, Ren Y, Xu J, Zhang L, Yu M, Zhang H, Yang H (2022) Effects of chemically functionalized TiO_2 nanoparticles on the UV-shielding characteristics of polymer-dispersed liquid crystals. Polym Adv Technol 33(5):1561–1568. https://doi.org/10.1002/pat.5621
19. Deng Y, Yang Y, Xiao Y, Xie HL, Lan R, Zhang L, Yang H (2023) Ultrafast switchable passive radiative cooling smart windows with synergistic optical modulation. Adv Funct Mater 33(35):2301319. https://doi.org/10.1002/adfm.202301319
20. Gao J, Yu P, Zhu S, Wen L, Wang X, Song W, Ge Y, He Z, Miao Z (2023) Polymer-dispersed liquid crystals with UV-shielding properties. Liq Cryst 50(13–14):2104–2113. https://doi.org/10.1080/02678292.2023.2229774
21. Lin H, Zhao Y, Jiao X, Gao H, Guo Z, Wang D, Luan Y, Wang L (2024) Preparation and application of polymer-dispersed liquid crystal film with step-driven display capability. Molecules 29(5):1109. https://doi.org/10.3390/molecules29051109
22. Chen X, He Z, Li C, Miao Z, Wang D, Luan Y, Li Y, Zhao Y (2022) Effects of formulation composition and CeO_2 nanoparticles doping on the morphologies of polymer spacer columns and electro-optical properties of PDLC. Mater Today Commun 31:103758. https://doi.org/10.1016/j.mtcomm.2022.103758
23. Wang D, Gu Y, Feng S, Yang W, Dai H, Xiao H, Han J (2023) Lignin-containing biodegradable UV-blocking films: a review. Green Chem 25:9020–9044. https://doi.org/10.1039/D3GC02908E
24. Li X, Li J, Shen X, Cao M, Wang Y, Zhang W, Xu Y, Ling Z, Chen S, Xu F (2024) Transparent cellulose/lignin composite films with adjustable haze and UV-blocking performance for light management. ACS Sustain Chem Eng 12(14):5427–5435. https://doi.org/10.1021/acssuschemeng.3c07076
25. Liu J, Moreno A, Chang J, Morsali M, Yuan J, Sipponen MH (2022) Fully biobased photothermal films and coatings for indoor ultraviolet radiation and heat management. ACS Appl Mater Interfaces 14(10):12693–12702. https://doi.org/10.1021/acsami.2c00718
26. Cui H, Zayat M, Parejo PG, Levy D (2008) Highly efficient inorganic transparent UV-protective thin-film coating by low temperature sol-gel procedure for application on heat-sensitive substrates. Adv Mater 20:65–68. https://doi.org/10.1002/adma.200701960
27. Mi R, Li T, Dalgo D, Chen C, Kuang Y, He S, Zhao X, Xie W, Gan W, Zhu J, Srebric J, Yang R, Hu L (2020) A clear, strong, and thermally insulated transparent wood for energy efficient windows. Adv Funct Mater 30(1):1907511. https://doi.org/10.1002/adfm.201907511
28. Hu X, Yu R, Wang F, Liu Z, Yang H, Chen C, Li Y, Noor N, Fei B (2023) Fabrication, functionalities and applications of transparent wood: a review. Adv Funct Mater 33(37):2303278. https://doi.org/10.1002/adfm.202303278
29. Yu Z, Yao Y, Yao J, Zhang L, Chen Z, Gao Y, Luo H (2017) Transparent wood containing Cs_xWO_3 nanoparticles for heat-shielding window applications. J Mater Chem A 5(13):6019–6024. https://doi.org/10.1039/C7TA00261K
30. Sun H, Bi H, Lin X, Cai L, Xu M (2020) Lightweight, anisotropic, compressible, and thermally-insulating wood aerogels with aligned cellulose fibers. Polymers 12(1):165. https://doi.org/10.3390/polym12010165
31. Farid T, Rafiq MI, Ali A, Tang W (2022) Transforming wood as next-generation structural and functional materials for a sustainable future. EcoMat 4(1):e12154. https://doi.org/10.1002/eom2.12154
32. Wu J, Liang Y, Xia C, Ma X, Fei B, Wu Y, Ge S, Lu J, Li J, Xia Z (2023) Laminated transparent woods with adjustable optical and enhanced mechanical properties. Adv Mater Technol 8(1):2200704. https://doi.org/10.1002/admt.202200704
33. Liu S, Tso CY, Lee HH, Du YW, Yu KM, Feng S-P, Huang B (2021) Self-densified optically transparent VO_2 thermochromic wood film for smart windows. ACS Appl Mater Interfaces 13(19):22495–22504. https://doi.org/10.1021/acsami.1c03803
34. Li Y, Yu S, Veinot JGC, Linnros J, Berglund L, Sychugov I (2017) Luminescent transparent wood. Adv Optical Mater 5(1):1600834. https://doi.org/10.1002/adom.201600834
35. Vasileva E, Li Y, Sychugov I, Mensi M, Berglund L, Popov S (2017) Lasing from organic dye molecules embedded in transparent wood. Adv Opt Mater 5(10):1700057. https://doi.org/10.1002/adom.201700057
36. Fu Q, Yan M, Jungstedt E, Yang X, Li Y, Berglund LA (2018) Transparent plywood as a load-bearing and luminescent biocomposite. Compos Sci Technol 164:296–303. https://doi.org/10.1016/j.compscitech.2018.06.001
37. Li Y, Fu Q, Yu S, Yan M, Berglund L (2016) Optically transparent wood from a nanoporous cellulosic template: combining functional and structural performance. Biomacromol 17(4):1358–1364. https://doi.org/10.1021/acs.biomac.6b00145
38. Li Y, Fu Q, Rojas R, Yan M, Lawoko M, Berglund L (2017) Lignin-retaining transparent wood. ChemSusChem 10(17):3445–3451. https://doi.org/10.1002/cssc.201701089
39. Qiu Z, Wang S, Wang Y, Li J, Xiao Z, Wang H, Liang D, Xie Y (2020) Transparent wood with thermo-reversible optical

properties based on phase-change material. Compos Sci Technol 200:108407. https://doi.org/10.1016/j.compscitech.2020.108407
40. Montanari Cl, Li Y, Chen H, Yan M, Berglund LA (2019) Transparent wood for thermal energy storage and reversible optical transmittance. ACS Appl Mater Interfaces 11(22):20465–20472. https://doi.org/10.1021/acsami.9b05525
41. Samanta A, Chen H, Samanta P, Popov S, Sychugov I, Berglund LA (2021) Reversible dual-stimuli-responsive chromic transparent wood biocomposites for smart window applications. ACS Appl Mater Interfaces 13(2):3270–3277. https://doi.org/10.1021/acsami.0c21369
42. Segal L, Creely JJ, Martin A Jr, Conrad C (1959) An empirical method for estimating the degree of crystallinity of native cellulose using the X-ray diffractometer. Text Res J 29(10):786–794. https://doi.org/10.1177/004051755902901003
43. Facca AG, Kortschot MT, Yan N (2006) Predicting the elastic modulus of natural fibre reinforced thermoplastics. Compos Pt A-Appl Sci Manuf 37(10):1660–1671. https://doi.org/10.1016/j.compositesa.2005.10.006
44. Frey M, Schneider L, Masania K, Keplinger T, Burgert I (2019) Delignified wood-polymer interpenetrating composites exceeding the rule of mixtures. ACS Appl Mater Interfaces 11(38):35305–35311. https://doi.org/10.1021/acsami.9b11105
45. Hu Y, Nakao T, Nakai T, Gu J, Wang F (2005) Dynamic properties of three types of wood-based composites. J Wood Sci 51:7–12. https://doi.org/10.1007/s10086-003-0614-y
46. Zhu M, Wang Y, Zhu S, Xu L, Jia C, Dai J, Song J, Yao Y, Wang Y, Li Y, Henderson D, Luo W, Li H, Minus ML, Li T, Hu L (2017) Anisotropic, transparent films with aligned cellulose nanofibers. Adv Mater 29(21):1606284. https://doi.org/10.1002/adma.201606284
47. Sun R, Tomkinson J, Mao FC, Sun XF (2001) Physicochemical characterization of lignins from rice straw by hydrogen peroxide treatment. J Appl Polym Sci 79(4):719–732. https://doi.org/10.1002/1097-4628(20010124)79:4<719::AID-APP170>3.0.CO;2-3
48. Xia Q, Chen C, Yao Y, He S, Wang X, Li J, Gao J, Gan W, Jiang B, Cui M, Hu L (2021) In situ lignin modification toward photonic wood. Adv Mater 33(8):2001588. https://doi.org/10.1002/adma.202001588
49. Nazim M, Kim JH (2020) Fluorescent N-doped graphene quantum dots embedded in transparent polymer films for photon-down-conversion applications. ACS Appl Nano Mater 3(3):2322–2335. https://doi.org/10.1021/acsanm.9b02436
50. Smith MJ, Malak ST, Jung J, Yoon YJ, Lin CH, Kim S, Lee KM, Ma R, White TJ, Bunning TJ, Lin Z, Tsukruk VV (2017) Robust, uniform, and highly emissive quantum dot–polymer films and patterns using thiol–ene chemistry. ACS Appl Mater Interfaces 9(20):17435–17448. https://doi.org/10.1021/acsami.7b03366
51. Mays RL, Pourhossein P, Savithri D, Genzer J, Chiechi RC, Dickey MD (2013) Thiol-containing polymeric embedding materials for nanoskiving. J Mater Chem C 1(1):121–130. https://doi.org/10.1039/C2TC00030J
52. Norland Optical Adhesive 63. https://norlandproducts.com/product/noa-63/. Accessed 30 Sept 2025
53. Höglund M, Johansson M, Sychugov I, Berglund LA (2020) Transparent wood biocomposites by fast UV-curing for reduced light-scattering through wood/thiol–ene interface design. ACS Appl Mater Interfaces 12(41):46914–46922. https://doi.org/10.1021/acsami.0c12505
54. Nasir N, Kumar S, Kim M, Nguyen VH, Suleman M, Park HM, Lee S, Kang D, Seo Y (2022) Effect of the photoinitiator concentration on the electro-optical properties of thiol–acrylate-based PDLC smart windows. ACS Appl Energy Mater 5(6):6986–6995. https://doi.org/10.1021/acsaem.2c00623
55. Jia C, Chen C, Mi R, Li T, Dai J, Yang Z, Pei Y, He S, Bian H, Jang SH, Zhu JY, Yang B, Hu L (2019) Clear wood toward high-performance building materials. ACS Nano 13(9):9993–10001. https://doi.org/10.1021/acsnano.9b00089
56. Frunza L, Kosslick H, Bentrup U, Pitsch I, Fricke R, Frunza S, Schönhals A (2003) Surface layer in composites containing 4-n-octyl-4`-cyanobiphenyl. FTIR spectroscopic characterization. J Mol Struct 651:341–347. https://doi.org/10.1016/S0022-2860(03)00110-8
57. Dangombe MS, Oladepo SA (2024) Investigation of solute-solvent interactions of 4`-alkyl-4-cyanobiphenyl liquid crystals using Raman spectroscopy. Spectroc Acta Pt A-Molec Biomolec Spectr 312:124067. https://doi.org/10.1016/j.saa.2024.124067
58. Zhang Z, Panov VP, Nagaraj M, Mandle RJ, Goodby JW, Luckhurst GR, Jones JC, Gleeson HF (2015) Raman scattering studies of order parameters in liquid crystalline dimers exhibiting the nematic and twist-bend nematic phases. J Mater Chem C 3(38):10007–10016. https://doi.org/10.1039/C5TC02174J
59. Qian Y, Qiu X, Zhu S (2016) Sunscreen performance of lignin from different technical resources and their general synergistic effect with synthetic sunscreens. ACS Sustain Chem Eng 4(7):4029–4035. https://doi.org/10.1021/acssuschemeng.6b00934
60. Deng Y, Feng X, Zhou M, Qian Y, Yu H, Qiu X (2011) Investigation of aggregation and assembly of alkali lignin using iodine as a probe. Biomacromolecules 12(4):1116–1125. https://doi.org/10.1021/bm101449b
61. Benmouna F, Daoudi A, Roussel F, Buisine JM, Coqueret X, Maschke U (1999) Equilibrium phase diagram of polystyrene and 8CB. J Polym Sci Pt B-Polym Phys 37(15):1841–1848. https://doi.org/10.1002/(SICI)1099-0488(19990801)37:15<1841::AID-POLB8>3.0.CO;2-3
62. Emelyanenko AV, Aya S, Sasaki Y, Araoka F, Ema K, Ishikawa K, Takezoe H (2011) Two transitions between isotropic and nematic phases in confined liquid crystals. Phys Rev E 84(4):041701. https://doi.org/10.1103/PhysRevE.84.041701
63. Horn RG (1978) Refractive indices and order parameters of two liquid crystals. J Phys Paris 39(1):105–109. https://doi.org/10.1051/jphys:01978003901010500

Publisher's Note Springer Nature remains neutral with regard to jurisdictional claims in published maps and institutional affiliations.